Data-Driven Chance-Constrained Optimal Gas-Power Flow Calculation: A Bayesian Nonparametric Approach

Data-Driven Chance-Constrained Optimal Gas-Power Flow Calculation: A Bayesian Nonparametric Approach

Jingyao Wang, Cheng Wang, *Member, IEEE*, Yile Liang, Tianshu Bi, *Senior Member, IEEE*, Miadreza Shafie-khah, *Senior Member, IEEE*, João P. S. Catalão, *Senior Member, IEEE*

***Abstract*—This paper proposes a data-driven chance-constrained optimal gas-power flow (OGPF) calculation method without any prior assumption on the distribution of uncertainties of wind power generation. The Gaussian mixture model is employed to fit the uncertainty distribution, where the Bayesian nonparametric Dirichlet process is adopted to tune the component number. To facilitate the online application of the proposed methods, an online-offline double-track distribution construction approach is established, where the frequency of training the relatively time-consuming Dirichlet process Gaussian mixture model can be reduced. On account of the quadratic gas consumption expression of gas-fired generators as well as the linear decision rule based uncertainty mitigation mechanism, the chance constraints would become quadratic ones with quadratic terms of uncertainties, which makes the proposed model more intractable. An equivalent linear separable counterpart is then provided for the quadratic chance constraints, after which the intractable chance constraints could be converted into traditional linear ones. The convex-concave procedure is used to crack the nonconvex Weymouth equation in the gas network and the auxiliary quadratic equalities. Simulation results on two test systems validate the effectiveness of the proposed methods.**

***Index Terms*—Chance-constrained optimization, Dirichlet process, Gaussian mixture model, optimal gas-power flow, wind power uncertainty.**

NOMENCLATURE

A. Sets and Indices

$b \in \mathcal{B}$	Electrical buses.
$c \in \mathcal{C}$	Gas compressors.
$d_p \in \mathcal{D}_p$	Electrical loads.
$d_g \in \mathcal{D}_g$	Gas loads.
$g \in \mathcal{G}$	Gas-fired generators.
$l_g \in \mathcal{L}_g$	Gas pipelines.
$l_p \in \mathcal{L}_p$	Power transmission lines.
$n \in \mathcal{N}$	Gas nodes.
$r \in \mathcal{R}$	Renewable generation (Wind farms).
$s \in \mathcal{S}$	Gas storage tanks.
$t \in \mathcal{T}$	Time periods.
$u \in \mathcal{U}$	Non-gas generators.
$w \in \mathcal{W}$	Gas wells.
T	Number of time periods.

B. Parameters

a'_g, a''_g, a'''_g	Energy conversion coefficients of gas-fired generators.
C_{d_p}/C_{d_g}	Electrical/gas load shedding costs.
C_s^+, C_s^-	Gas storage charge/discharge costs.
C_u^+, C_u^-	Upward/downward reserve cost of non-gas generators.
C_w	Gas well production costs.
$P_{d_p t}$	Electrical load demands.
$\overline{P}_g/\underline{P}_g$	Generation capacity of gas-fired generators.
P_g^+, P_g^-	Ramping capacity of gas-fired generators.
$\overline{P}_{l_p}$	Upper limits of transmission lines.
$\overline{P}_u/\underline{P}_u$	Generation capacity of non-gas generators.
P_u^+, P_u^-	Ramping capacity of non-gas generators.
$\hat{p}_{rt}$	Forecasted outputs of wind generation.
$Q_{d_g t}$	Gas load demands.
$\overline{Q}_s/\underline{Q}_s$	Max/Min gas storage volume.
Q_s^+, Q_s^-	Charge/discharge rate of gas storage.
$\overline{Q}_w/\underline{Q}_w$	Max/Min production of gas wells.
$\overline{Z}_n/\underline{Z}_n$	Gas node pressure limits.
α_{gt}/α_{ut}	Affine coefficients of gas-fired/non-gas generators.
β_c	Fuel consumption coefficients of compressors.
χ_{l_g}	Weymouth equation coefficients.
ε	Violation probability of chance constraints.
η_{l_g}	Line pack coefficients.
$\lambda_{gt}/\lambda_{ut}$	Operating status of gas-fired/non-gas generators.
$\pi_{d_p l_p}$	Power transfer distribution factor of electrical loads.
$\pi_{g l_p}/\pi_{r l_p}/\pi_{u l_p}$	Power transfer distribution factors of gas-fired/renewable/non-gas generators.
$\Gamma_{c l_g}$	Compression factor.

C. Decision Variables

$m_{l_g t}$	Average gas mass of pipelines.
$p_{d_p t}/q_{d_g t}$	Electrical/gas load shedding.
p_{gt}/p_{ut}	Outputs of gas-fired/non-gas generators.
$p_{l_p t}$	Actual power flow.
q_{gt}	Gas consumption of gas-fired generators.
$q_{l_g t}^+, q_{l_g t}^-$	In-/out-flows of gas pipelines.
q_{st}	Gas storage volume.
q_{st}^+, q_{st}^-	Base-case storage charge/discharge.
q_{wt}	Gas production of gas wells.
r_{gt}^+, r_{gt}^-	Up-/down-ward reserves of gas-fired generators.
r_{st}^+, r_{st}^-	In-/out-flow bound of uncertain gas storage.
r_{ut}^+, r_{ut}^-	Up-/down-ward reserves of non-gas generators.
z_{nt}	Gas node pressure.
θ_{bt}	Bus angles.

D. Random Variables

$\tilde{p}_{rt}$	Actual outputs of wind generation.
$\Delta\tilde{q}_{gt}$	Gas consumption deviations of gas-fired generators.
$\Delta\tilde{q}_{st}$	Gas storage outputs deviations.
Ω_t	Sum of forecast deviations of wind power.

I. Introduction

INTEGRATED energy system (IES) is one of the most promising forms of future energy systems, where the energy consumption can be carried out in a more efficient, reliable and eco-friendly manner [1]. Based on the energy coupling modes and geographic sizes, quite a few variations have been developed under the concept of the IES, such as the integrated electric-gas system (IEGS) and the integrated electric-heat system (IEHS). Due to the technical breakthroughs in shale gas mining and turbine technologies as well as emerging power-to-gas (P2G) facilities [2], the IEGS has been driving the attentions from academic communities in recent decades, including the operation [3], planning [4] and marketing [5] perspectives.

Optimal gas-power flow (OGPF) is one of the most fundamental problems in the area of IEGS operation, which has been addressed by many inspiring works. A steady-state OGPF model was proposed in [6], where the computational challenging Weymouth equations were replaced with their mixed integer linear program (MILP) based approximation. In [7], the simplified gas flow dynamics was incorporated in the OGPF model, which can still be converted into a tractable problem by employing the mixed integer based piecewise linearization. To alleviate the computation burden brought by the large-scale of auxiliary binary variables, a convex optimization based solution procedure is devised in [8] for the OGPF with predetermined gas flow directions, where only a series of second-order cone programs (SOCPs) is require to be solved.

With the fast development of the renewable power generation, such as wind and photovoltaic power generation, new challenges have been imposed on the operation of the IEGS, as the original variability and uncertainty in the electrical power network would be transmitted to the gas network via gas-fired generators and P2G facilities, giving rise to the urgent need of designing effective decision-making frameworks for the OGPF problem. The two important steps of solving the OGPF with uncertainties is to model the uncertainty properly and to select a proper model to characterize the impacts of uncertainties on the OGPF problem. In recent years, data-driven uncertainty modeling methods have been drawn more and more attention, including the interval model [9], [10], [11], uncertainty set model [12], analytical distribution model [13], [14], scenario set model [15] and fuzzy set model [16]. Accordingly, various advanced decision-making frameworks and optimization methods have been developed and applied along with the aforementioned uncertainty models, such as the interval optimization [11], robust optimization [17], chance-constrained programming [14], scenario-based stochastic optimization [15] and distributionally robust optimization [18] methods. In what follows, their applications in OGPF problem would be reviewed.

In [15], a scenario-based stochastic OGPF model is proposed considering the electricity demand response mechanism. To overcome the inherent defect of the scenario-based method, which is the unguaranteed operation feasibility of the solution w.r.t. unselected scenarios, robust optimization becomes a popular choice for OGPF problem with uncertainties. A two-stage robust OGPF model is constructed in [17], where the Weymouth equations are approximated by second-order cone (SOC) constraints and the indirect adverse effect of wind generation uncertainty is mitigated locally by distributed gas storages. Based on the work of [17], the linear decision rule for controllable generators and a multi-slack-node scheme for gas network regulation are employed in [19], which can not only make the two-stage decision-making structure reduce to a single-level one but also guarantee the solution feasibility. However, the OGPF solution generated from robust models may be conservative.

Another viable way to capture the impacts of uncertainties on the OGPF problem is chance-constrained modeling, where each constraint containing random variables has a probabilistic guarantee to be satisfied and the overall framework can be extended to a fully data-driven one [20]. In [14], a chance-constrained optimization model for the multi-energy flow calculation is established, where the probabilistic distribution functions (PDFs) for solar and wind generation outputs are set as Beta and Weibull distributions, respectively. In addition, multivariate Gaussian [13] and Chi-square [21] distributions have been selected as prior distributions for uncertainty modeling in chance-constrained optimal power flow (CC-OPF) problems. To overcome the subjectivity of choosing the prior distribution for the uncertainties, a distributionally robust chance-constrained OGPF model is proposed in [18], in which the probabilistic guarantee holds for the family of candidate distributions with the same mean and covariance as the reference one formed by a sample set. According to [22] and [23], the consumed gas of gas-fired generators can be approximated by quadratic functions w.r.t. their outputs, which would increase the difficulty of solving chance-constrained OGPF models, as nontrivial quadratic random variable terms would appear in the chance constraints describing the impacts of renewable generation uncertainties on gas systems.

Gaussian mixture model (GMM) is the distribution with multiple Gaussian components and supposed to fit arbitrary data samples with a given number of Gaussian components theoretically. With the development of data measurement and storage techniques, huge amount of historical data of uncertainty realization would be available, which would facilitate the application of data-driven uncertainty modeling methods, such as GMM. Recent applications of GMM on the CC-OPF demonstrate its fitting ability and better posterior results than Monte Carlo simulation, multivariate Gaussian and other common distributions [24], [25]. However, the number of components in GMM needs to be predetermined, which indicates overfitting or underfitting may occur if the component number is chosen inappropriately.

Fortunately, a Bayesian nonparametric method named Dirichlet process mixture model (DPMM) is developed to determine the component number of mixture models by a posterior process [26]. In [27], DPMM is adopted to set the component numbers for basic uncertainty sets in the robust unit commitment problem. In [28], a variational Bayesian interference (VBI) based DPMM method is applied in wind generation uncertainty modeling, overcoming the time-consuming shortcoming of Markov chain Monte Carlo

(MCMC) based one. However, DPMM is solved by posterior calculation and the time cost is inevitable, whatever on account of MCMC or faster VBI. For high-dimension and large-size data sets, the time-consuming issue will become more prominent [29], especially in the online scenario.

One possible avenue to mitigate the time-consuming issue of the DPGMM based fitting method is to design a double-track fitting method, which includes an online track and an offline one. In fact, the online-offline double-track framework has been employed in many applications of the power system operation. In [30], the framework is designed with offline training and online prediction in online voltage stability assessment, where the offline part is to establish the model based on database and the online part is updated adaptive to system changes. To overcome the difficulties of online learning model update and offline training data preparation, an active learning solution is proposed to enhance existing applications by actively interacting with the online prediction and offline training process in [31]. Based on the mechanism of knowledge transition and extension, an online search method for representative risky fault chains is proposed in [32], where the knowledge in past runs is accumulated offline and then applied online. Likewise, other works of online-offline application are also based on the online decision with the offline reference [33], [34], with a concern the online model cannot fully represent the real scenario. However, the online-offline double-track framework has not been applied to data-driven PDF fitting problems.

In this paper, a Bayesian nonparametric chance-constrained optimal gas-power flow (CC-OGPF) model along with its solution procedure are proposed considering the uncertainty of wind generation outputs. Compared with existing works, the salient features are summarized as follows.

1) An online-offline double-track approach is proposed to fit the PDF and cumulative distribution function (CDF) of the wind generation outputs uncertainty, which is suitable for rolling horizon OGPF calculation with high-dimension and large-size data sets. In the offline track, the relatively time-consuming Dirichlet process Gaussian mixture model (DPGMM) is employed to determine the reference value of Gaussian distribution component number; while in the online track, GMM with different component numbers around the latest reference value are performed and the fitted distribution with the minimum Akaike information criterion (AIC) value is selected as the candidate distribution for chance constraint conversion.

2) The proposed model is not readily solvable due to the intractable quadratic chance constraints. An equivalent form is established for the quadratic chance constraints, where the decision and random variables become linear separable. Then, the reformulated chance constraints are converted into tractable ones with parameterized quantiles of the multivariate GMM according to the results of [35], and the quantiles can be obtained by the inverse of multiple CDF superposition function. Hereinafter, the original problem is reformulated as a computational challenging nonlinear program. A local optimal and feasible solution can be obtained by solving a series of mixed integer second-order cone program (MISOCP) based approximation model sequentially.

II. Mathematical Formulation

A. Objective Function

The objective function of the proposed CC-OGPF model is to minimize the total out-of-pocket costs of the IEGS, shown as (1) [6], [7], [36].

$$F=\min\sum_{t\in\mathcal{T}}\left[\begin{array}{l}\sum\limits_{u\in\mathcal{U}}C_u\left(p_{ut}\right)+\sum\limits_{u\in\mathcal{U}}C_u^+r_{ut}^+\\+\sum\limits_{u\in\mathcal{U}}C_u^-r_{ut}^-+\sum\limits_{w\in\mathcal{W}}C_wq_{wt}\\+\sum\limits_{s\in\mathcal{S}}C_s^+\max\left\{0,q_{st}^+-q_{st}^-+r_{st}^+\right\}\\+\sum\limits_{s\in\mathcal{S}}C_s^-\max\left\{0,q_{st}^--q_{st}^++r_{st}^-\right\}\\+\sum\limits_{d_g\in\mathcal{D}_g}C_{d_g}q_{d_gt}+\sum\limits_{d_p\in\mathcal{D}_p}C_{d_p}p_{d_pt}\end{array}\right]. \quad (1)$$

In (1), the first term represents the generation costs of the non-gas generators, where $C_u(\cdot)$ is a quadratic function; the second and third terms are the upward and downward reserve costs of the non-gas generators, respectively; the fourth term denotes the production costs of gas wells; the fifth and sixth terms express the bidirectional regulation costs of gas storages, including both the base-case and worst-case scenarios; the last two terms give the penalties for unserved gas and electrical loads, respectively. It should be noted that the $\max\{\}$ operator in (1) is convexity-preserving, which can be easily eliminated by introducing a non-negative auxiliary variable and a linear constraint [37].

B. Deterministic Constraint Modeling

The constraints of the CC-OGPF model could be classified into deterministic and chance constraints in terms of the appearance of random variables. Hereinafter, the constraints with no random variable are denoted as deterministic constraints.

1) Power system operation constraints: Equations (2a)-(2g) summarize the deterministic constraints of electric power system [6], [7]. Specifically, equation (2a) gives the generation capacity of gas-fired and non-gas generators; equation (2b) describes the ranges of committed reserves considering the base-case operation points of generators; equations (2c) and (2d) impose the extreme requirements of ramping capability of generators with the consideration of reserve utilization; equation (2e) states the system-level power balancing condition; equation (2f) demonstrates the upper bound of the power flow in each transmission line; equation (2g) guarantees the non-negativity of the electrical load shedding.

$$\lambda_{\{\cdot\}t}\underline{P}_{\{\cdot\}}\le p_{\{\cdot\}t}\le\lambda_{\{\cdot\}t}\overline{P}_{\{\cdot\}},\{\cdot\}=\{g,u\},\forall g,\forall u,\forall t, \quad (2a)$$

$$\begin{aligned}0\le r_{\{\cdot\}t}^+\le\lambda_{\{\cdot\}t}\overline{P}_{\{\cdot\}}-p_{\{\cdot\}t},\\0\le r_{\{\cdot\}t}^-\le p_{\{\cdot\}t}-\lambda_{\{\cdot\}t}\underline{P}_{\{\cdot\}},\\\{\cdot\}=\{g,u\},\forall g,\forall u,\forall t,\end{aligned} \quad (2b)$$

$$\begin{aligned}&\left(p_{\{\cdot\},t+1}+r_{\{\cdot\},t+1}^+\right)-\left(p_{\{\cdot\}t}-r_{\{\cdot\}t}^-\right)\le\lambda_{\{\cdot\}t}P_{\{\cdot\}}^+\\&+(1-\lambda_{\{\cdot\}t})\overline{P}_{\{\cdot\}},\{\cdot\}=\{g,u\},\forall g,\forall u,\forall t,\end{aligned} \quad (2c)$$

$$\begin{aligned}&\left(p_{\{\cdot\}t}+r_{\{\cdot\}t}^+\right)-\left(p_{\{\cdot\},t+1}-r_{\{\cdot\},t+1}^-\right)\le\lambda_{\{\cdot\},t+1}P_{\{\cdot\}}^-\\&+(1-\lambda_{\{\cdot\},t+1})\overline{P}_{\{\cdot\}},\{\cdot\}=\{g,u\},\forall g,\forall u,\forall t,\end{aligned} \quad (2d)$$

$$\sum_g p_{gt}+\sum_u p_{ut}+\sum_r\hat{p}_{rt}=\sum_{d_p}(P_{d_pt}-p_{d_pt}),\forall t, \quad (2e)$$

$$-\overline{P}_{l_p} \le p_{l_pt} \le \overline{P}_{l_p}, p_{l_pt} = \sum_r \pi_{rl_p}\hat{p}_{rt} + \sum_u \pi_{ul_p}p_{ut} + \sum_g \pi_{gl_p}p_{gt} + \sum_{d_p} \pi_{d_pl_p}\left(P_{d_pt} - p_{d_pt}\right), \forall l_p, \forall t, \tag{2f}$$

$$0 \le p_{d_pt} \le P_{d_pt}, \forall d_p, \forall t. \tag{2g}$$

2) Natural gas system operation constraints: Similarly, equations (3a)-(3l) give the deterministic constraints of natural gas network [6], [7], [36]. Equation (3a) limits the gas production of gas wells; equations (3b) and (3c) illustrate the gas storage model, which includes the storage volume capacity constraint (3b) and the maximum gas charge/discharge limit (3c); equation (3d) depicts the nodal gas balancing condition, where $\Phi_w(n), \Phi_s(n), \Phi_g(n), \Phi_{d_g}(n)$ represent the sets of gas wells, storage tanks, gas-fired generators and gas loads connected to node n, and $\Phi_{l_g^1}(n), \Phi_{l_g^2}(n)$ represent the set of pipelines whose initial or terminal node is node n; equation (3e) is the Weymouth equation [7], which describes the relationship between gas node pressure and the average pipeline flow; equation (3f) shows the nodal pressure limit; equation (3g) is the simplified gas compressor model [7], [36], where $\Phi_{l_g}(c)$ represents the set of gas pipelines equipped with compressors; equation (3h) indicates the relationship between in-/out-flow of a pipeline with a compressor, where the fuel consumption rate is usually subject to $[0.03,\ 0.05]$; equation (3i) provides the simplified line pack model [36], which specifies the relationship between gas mass and nodal pressures; equation (3j) expresses the charging and discharging of line pack during operation; equation (3k) represents the gas consumption of gas-fired generators [38], where $f_g(\cdot)$ denotes the gas consumption function; equation (3l) guarantees the non-negativity of the gas load shedding.

$$\underline{Q}_w \le q_{wt} \le \overline{Q}_w, \forall w, \forall t, \tag{3a}$$

$$\underline{Q}_s \le q_{st} = q_{s,t-1} + q_{st}^+ - q_{st}^- \le \overline{Q}_s, \forall s, \forall t, \tag{3b}$$

$$0 \le q_{st}^+ \le Q_s^+, 0 \le q_{st}^- \le Q_s^-, \forall s, \forall t, \tag{3c}$$

$$\sum_{l_g \in \Phi_{l_g^2}(n)} q_{l_gt}^- - \sum_{l_g \in \Phi_{l_g^1}(n)} q_{l_gt}^+ + \sum_{w \in \Phi_w(n)} q_{wt} - \sum_{g \in \Phi_g(n)} q_{gt} = \sum_{d_g \in \Phi_{d_g}(n)} \left(Q_{d_gt} - q_{d_gt}\right) - \sum_{s \in \Phi_s(n)} \left(q_{st}^- - q_{st}^+\right), \forall n, \forall t, \tag{3d}$$

$$\bar{q}_{l_gt}\left|\bar{q}_{l_gt}\right| = \chi_{l_g}\left(z_{l_g^1t}^2 - z_{l_g^2t}^2\right), \bar{q}_{l_gt} = \left(q_{l_gt}^- + q_{l_gt}^+\right)/2, \forall l_g, \forall t, \tag{3e}$$

$$\underline{Z}_n \le z_{nt} \le \overline{Z}_n, \forall n, \forall t, \tag{3f}$$

$$z_{l_g^2t} \le \Gamma_{cl_g} z_{l_g^1t}, l_g \in \Phi_{l_g}(c), \forall c, \forall t, \tag{3g}$$

$$(1-\beta_c)q_{ct}^+ - q_{ct}^- = 0, \forall c, \forall t, \tag{3h}$$

$$m_{l_gt} = \eta_{l_g}\left(z_{l_g^1t} + z_{l_g^2t}\right), \forall l_g, \forall t, \tag{3i}$$

$$m_{l_gt} = m_{l_g,t-1} + q_{l_gt}^+ - q_{l_gt}^-, \forall l_g, \forall t, \tag{3j}$$

$$q_{gt} = f_g(p_{gt}) = a_g'\lambda_{gt} + a_g''p_{gt} + a_g'''(p_{gt})^2, \forall g, \forall t, \tag{3k}$$

$$0 \le q_{d_gt} \le Q_{d_gt}, \forall d_g, \forall t. \tag{3l}$$

C. Chance-constrained Modeling

To mitigate the deviation of actual outputs of wind generation from their predicted values, reserves are committed from both gas-fired and non-gas generators and utilized based on the linear decision rule [13]. Meanwhile, the hard constraints with random variables are relaxed as chance constraints, as shown in (4a)-(4d), in order to reduce the conservativeness of the OGPF solution.

$$\Delta\tilde{p}_{rt} := \tilde{p}_{rt} - \hat{p}_{rt}, \forall r,\ \Omega_t := \sum_{r \in \mathcal{R}} \left(\tilde{p}_{rt} - \hat{p}_{rt}\right), \forall t, \tag{4a}$$

$$\Pr\left(-\alpha_{\{\cdot\}t}\Omega_t \le r_{\{\cdot\}t}^+\right) \ge 1-\varepsilon, \{\cdot\} = \{g,u\}, \forall g, \forall u, \forall t, \tag{4b}$$

$$\Pr\left(\alpha_{\{\cdot\}t}\Omega_t \le r_{\{\cdot\}t}^-\right) \ge 1-\varepsilon, \{\cdot\} = \{g,u\}, \forall g, \forall u, \forall t, \tag{4c}$$

$$\Pr\left(\begin{array}{l}\sum\limits_{r \in \mathcal{R}} \pi_{rl_p}\Delta\tilde{p}_{rt} + \sum\limits_{u \in \mathcal{U}} \pi_{ul_p}(-\alpha_{ut}\Omega_t) \\ + \sum\limits_{g \in \mathcal{G}} \pi_{gl_p}(-\alpha_{gt}\Omega_t) + p_{l_pt} \le \overline{P}_{l_p}\end{array}\right) \ge 1-\varepsilon,$$

$$\Pr\left(\begin{array}{l}\sum\limits_{r \in \mathcal{R}} \pi_{rl_p}\Delta\tilde{p}_{rt} + \sum\limits_{u \in \mathcal{U}} \pi_{ul_p}(-\alpha_{ut}\Omega_t) \\ + \sum\limits_{g \in \mathcal{G}} \pi_{gl_p}(-\alpha_{gt}\Omega_t) + p_{l_pt} \ge -\overline{P}_{l_p}\end{array}\right) \ge 1-\varepsilon, \quad \forall l_p, \forall t. \tag{4d}$$

In this formulation, (4a) defines the individual and total deviation of wind generation outputs; (4b) and (4c) manifest the outputs adjustment of generators, i.e. $-\alpha_{\{\cdot\}t}\Omega_t$, should fall in the scope of the committed reserves with the probability higher than $(1-\varepsilon)$; (4d) indicates the overload probability of each transmission line should not exceed ε considering the deviation of wind generation outputs as well as utilization of reserves.

Considering the affine rule of reserve regulation, the actual outputs of gas-fired generators become random along with the outputs of wind generation. Consequently, the uncertainty of wind generation outputs in the power network would be transmitted to the gas network via the energy conversion devices, which are the gas-fired generators in this work, considering the mapping between the outputs of gas-fired generators and their gas consumption. In fact, the deviation of actual gas consumption of gas-fired generators from their base-case values could be easily obtained by parameterizing (3k) with p_{gt} and $(p_{gt} - \alpha_{gt}\Omega_t)$, respectively, as shown in (5).

$$\Delta\tilde{q}_{gt} = a_g'''\alpha_{gt}^2\Omega_t^2 - a_g''\alpha_{gt}\Omega_t - 2a_g'''\alpha_{gt}\Omega_t p_{gt}, \forall g, \forall t. \tag{5}$$

Considering the relative slow gas flow dynamics, the uncertain gas fuel demands of the gas-fired generators may not be fully mitigated by merely regulating the outputs of gas wells. Therefore, gas storages are usually equipped at the same gas node as the gas-fired generators so as to buffer the impacts of gas fuel uncertainties on the gas network operation [17], [19], which is captured by (6).

$$\Delta\tilde{q}_{st} = \Delta\tilde{q}_{gt}, s \in \Phi_s(g), \forall g, \forall t. \tag{6}$$

As the gas reserve providers in the gas network, the operation of gas storages should obey the charging/discharging rate and capacity constraints under the worst-case reserve utilization scenarios, which are depicted by (7) and (8), respectively.

$$0 \le r_{st}^+ \le Q_s^+ - q_{st}^+,\ 0 \le r_{st}^- \le Q_s^- - q_{st}^-, \forall s, \forall t, \tag{7}$$

$$\underline{Q}_s \le q_{st} - \sum_{\tau=1}^{t} r_{s\tau}^-,\ q_{st} + \sum_{\tau=1}^{t} r_{s\tau}^+ \le \overline{Q}_s, \forall s, \forall t. \tag{8}$$

Similarly, the gas reserve adequacy constraints are relaxed

as chance constraints, as shown in (9).

$$\Pr\left(\Delta\tilde{q}_{st} \le r_{st}^{-}\right) \ge 1-\varepsilon, \forall s, \forall t, \tag{9a}$$

$$\Pr\left(\Delta\tilde{q}_{st} \ge -r_{st}^{+}\right) \ge 1-\varepsilon, \forall s, \forall t. \tag{9b}$$

As the uncertainty of gas storage outputs adjustment originate from the uncertainties of wind generation outputs, $\Delta\tilde{q}_{st}$ in (9) can be substituted by the expressions containing Ω_t in (5) and (6), and the chance constraints in the gas network can be reformulated as

$$\Pr\left(a_g'''\alpha_{gt}^2\Omega_t^2 - a_g''\alpha_{gt}\Omega_t - 2a_g'''\alpha_{gt}\Omega_t p_{gt} \le r_{st}^{-}\right) \ge 1-\varepsilon, \quad s \in \Phi_s(g), \forall g, \forall t, \tag{10a}$$

$$\Pr\left(a_g'''\alpha_{gt}^2\Omega_t^2 - a_g''\alpha_{gt}\Omega_t - 2a_g'''\alpha_{gt}\Omega_t p_{gt} \ge -r_{st}^{+}\right) \ge 1-\varepsilon, \quad s \in \Phi_s(g), \forall g, \forall t. \tag{10b}$$

It should be noted that (10) admits a set of nontrivial constraints, owing to the existence of nonlinear terms of random variables.

Remark: It should be highlighted that the gas load uncertainty could be considered and its impacts on the gas network operation would also be described by chance constraints. New variables should be defined as follows: $\tilde{Q}_{d_g t}$ represents the actual gas load demands, $\Delta\tilde{Q}_{d_g t}$ represents the gas load deviation from the predicted value $Q_{d_g t}$, r_{st}^{g+} and r_{st}^{g-} represent the committed reserve for gas load uncertainty, r_{st}^{p+} and r_{st}^{p-} represent the committed reserve for the uncertainty of gas-fired generator fuel consumption.

The chance constraints brought by the gas load uncertainty model are shown in (11).

$$\Pr\left(\Delta\tilde{Q}_{d_g t} \le r_{st}^{g-}\right) \ge 1-\varepsilon, \forall s, \forall t, \tag{11a}$$

$$\Pr\left(\Delta\tilde{Q}_{d_g t} \ge -r_{st}^{g+}\right) \ge 1-\varepsilon, \forall s, \forall t. \tag{11b}$$

Accordingly, the chance constraints (9) originated from the gas demand uncertainty of gas-fired generators should be modified as (12).

$$\Pr\left(\Delta\tilde{q}_{st} \le r_{st}^{p-}\right) \ge 1-\varepsilon, \forall s, \forall t, \tag{12a}$$

$$\Pr\left(\Delta\tilde{q}_{st} \ge -r_{st}^{p+}\right) \ge 1-\varepsilon, \forall s, \forall t. \tag{12b}$$

In addition, the following auxiliary constraints for the gas reserves should be considered.

$$\begin{aligned} &r_{st}^{g+} + r_{st}^{p+} = r_{st}^{+}, r_{st}^{g-} + r_{st}^{p-} = r_{st}^{-}, \\ &r_{st}^{g+}, r_{st}^{p+}, r_{st}^{g-}, r_{st}^{p-} \ge 0, \ \forall s, \forall t. \end{aligned} \tag{13}$$

III. Solution Methodology

Though the CC-OGPF model has been established in Section II, three major challenges need to be addressed before importing the proposed model to commercial solvers. (1) How to construct a precise and analytical PDF for the uncertainty? (2) How to equivalently convert the chance constraints, especially the quadratic ones, into normal ones? (3) How to solve the reformulated CC-OGPF model considering the computational challenging Weymouth equations? These three challenges would be overcome in the three subsections of Section III, whose layout is shown in Fig.1.

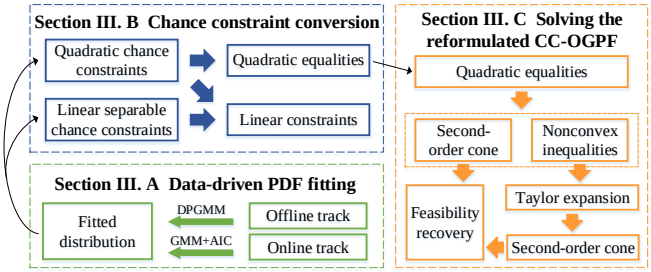

Fig. 1. Layout of Section III.

A. DPGMM based Distribution Construction

As aforementioned, GMM could be adopted to generate a candidate distribution for the uncertainties. However, the component number for GMM training, which is a crucial parameter on the performance of the training results, has to be predetermined. For the ease of analysis, the general expression for GMM for multivariate vector $\boldsymbol{X}$ is presented as follows.

$$\mathrm{GMM}_{\boldsymbol{X}} = \sum_{i=1}^{I} \pi_i N_i\left(\boldsymbol{\mu}_i, \boldsymbol{\Sigma}_i\right), \sum_{i=1}^{I} \pi_i = 1, \tag{14}$$

where I and i are the component number and index, respectively; π_i denotes the component weight; N_i represents the multivariate Gaussian distribution with $\boldsymbol{\mu}_i$ and $\sum_i$ as the mean and the covariance, respectively.

Dirichlet process (DP) is a random process for the Bayesian nonparametric model, which is commonly used for the prior of DPGMM. It can be viewed as a probability distribution over the space of distributions [39] to draw the distribution as a sample, while its margin distribution of finite dimensions is the Dirichlet distribution. Suppose a random distribution G follows the DP denoted as $G \sim DP(\alpha, G_0)$, where α represents the concentration parameter, G_0 is a base measurement over space Θ. For any atom location $(\theta_1, \cdots, \theta_i)$ of Θ, holds $(G(\theta_1), \cdots, G(\theta_i)) \sim Dirichlet(\alpha G_0(\theta_1), \cdots, \alpha G_0(\theta_i))$, where $Dirichlet$ represents the Dirichlet distribution.

To overcome the subjectivity while choosing the component number of the Gaussian mixture model, a DPGMM based distribution construction method is proposed. Following the stick-breaking process, the random sampling from DP is supposed to be $G = \sum_i^{\infty} \pi_i \delta_{\theta_i}$, where δ_{θ_i} is Dirac delta measurement and $\pi_i = \beta_i \Pi_{j=1}^{i-1}(1-\beta_j)$ is the weight on atom $\theta_i \in \Theta$, $\beta_j \sim Beta(1, \alpha)$, the atom location θ_i subjects to base probability measurement G_0 [40]. Drawing from DP with hierarchical label l_k, the formulation of DPGMM is presented in equations (15a)-(15c).

$$\{\pi_i, \theta_i\}_{i=1}^{\infty} \sim DP(\alpha, G_0), \tag{15a}$$

$$l_k \sim Cate\left(\{\pi_i\}_{i=1}^{\infty}\right), \tag{15b}$$

$$o_k \sim F\left(\theta_{l_k}\right). \tag{15c}$$

In this formulation, DP denotes the Dirichlet process; G_0 is the inverse Wishart distribution; α represents the concentration parameter and determines the distribution of π_i; θ_i consists of a mean vector $\boldsymbol{\mu}_i$ and a covariance matrix $\boldsymbol{\Sigma}_i$; $Cate$ is a multinomial distribution; l_k represents the hierarchical label of observations; k is the hierarchical index; F is the likelihood of θ_{l_k}, which is a multivariate Gaussian

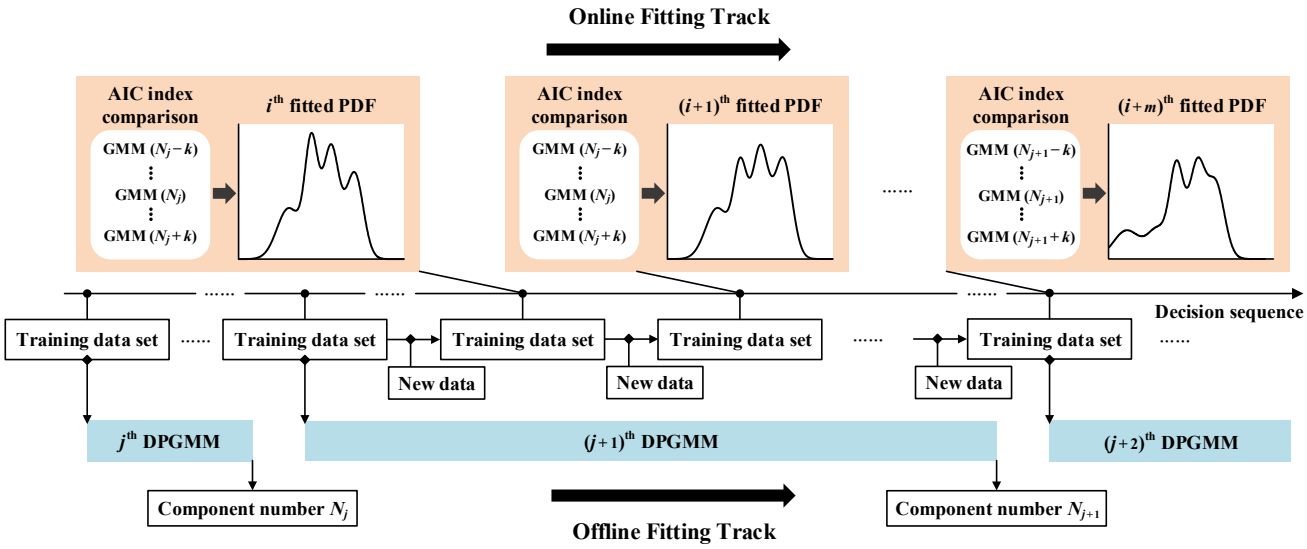

Fig. 2. Schematic diagram of the proposed double-track PDF fitting approach.

distribution; o_k represents the datapoint in the dataset of $F(\theta_{l_k})$.

By performing DPGMM, the number, mean vectors and covariance matrices of the multivariate Gaussian distributions N_i can be obtained. It should be noted that it would be much more time-consuming if DPGMM is employed to construction the uncertainty distribution instead of GMM. The reason is that additional sampling procedure has to be performed in the posterior process of DPGMM. Common sampling methods include Markov chain Monte Carlo (MCMC) and automatic differentation variational inference (ADVI), where the latter is much faster. However, DPGMM with ADVI could still be time-consuming while the size and dimensionality of the data set are huge, making it less attractive to real-world online applications. Therefore, an online-offline double-track approach is proposed to fit the distributions of the uncertainties combining the benefits of GMM and DPGMM, whose schematic diagram is shown in Fig.2. The solution process is shown as Algorithm 1.

In the offline track of proposed PDF fitting approach, a series of DPGMMs are sequentially performed with the latest data set, where each DPGMM could provide a reference value of the component number, denoted as N_j. Simultaneously, a series of GMMs are generated in parallel with the given component number range $[N_j-k, N_j+k]$ in the online track, and the GMM with the minimum AIC value would be selected to construct the uncertainty distribution [41], [42]. Especially, this approach is also effective for the uncertainty characterization of wind farms, load demands, photovoltaic generation outputs, and the line ratings of overhead lines.

Algorithm 1 Online-offline double-track PDF fitting.

1: **Initialization** Prepare the initial training data set. Set value for k. Set $i = 1$ and $j = 1$. Set the online track activation flag $\Lambda = 0$.

2: **Offline**
i. Update the training data set.
ii. Run j^{th} DPGMM. Record the component number N_j. Set $\Lambda = 1$. Send N_j to the online track.
iii. Set $j = j + 1$ and repeat **Step 2.i** of the offline track.
Online
i. If $\Lambda = 1$, go to **Step 2.ii** of the online track; otherwise, go to **Step 2.i** of the online track.
ii. Update the training data set and N_j.
iii. Run a series of GMMs with component range $[N_j-k,\ N_j+k]$. Calculate the AIC index for the fitted GMMs. Select the GMM with the least AIC index as the fitted PDF for i^{th} decision.
iv. Set $i = i + 1$ and repeat **Step 2.ii** of the online track.

B. Reformulations of Chance Constraints with DPGMM

The chance constraints in the proposed model include two parts, namely (4b)-(4d) and (10a)-(10b), where the former part admits a relatively simple structure, as the random and decision variables are linear separable, and the latter one is more complex, due to the appearance of continuous linear products of random and decision variables as well as the quadratic terms of random variables.

Using the method of completing square, equivalent forms of (10a)-(10b) can be derived as

$$\Pr\left(\frac{r_{st}^{-}}{a_g'''}+\left(p_{gt}+\frac{a_g''}{2a_g'''}\right)^2 \geq \left(p_{gt}-\alpha_{gt}\Omega_t+\frac{a_g''}{2a_g'''}\right)^2\right) \geq 1-\varepsilon, s\in\Phi_s(g), \forall g, \forall t, \tag{16a}$$

$$\Pr\left(\left(p_{gt}-\alpha_{gt}\Omega_t+\frac{a_g''}{2a_g'''}\right)^2 \geq \left(p_{gt}+\frac{a_g''}{2a_g'''}\right)^2-\frac{r_{st}^{+}}{a_g'''}\right) \geq 1-\varepsilon, s\in\Phi_s(g), \forall g, \forall t. \tag{16b}$$

Proposition 1. *The linear separable chance constraints (17a)-(17b) together with the corresponding auxiliary constraints (17c)-(17d) are equivalent to (10a)-(10b).*

$$\Pr\left(p_{gt}-\alpha_{gt}\Omega_t+a_g''/2a_g''' \leq h_{gt}^{-}\right) \geq 1-\varepsilon, \forall g, \forall t, \tag{17a}$$

$$\Pr\left(p_{gt}-\alpha_{gt}\Omega_t+a_g''/2a_g'''\geq h_{gt}^{+}\right)\geq 1-\varepsilon,\forall g,\forall t, \quad (17b)$$

$$(h_{gt}^{-})^2=r_{st}^{-}/a_g'''+\left(p_{gt}+a_g''/2a_g'''\right)^2, s\in\Phi_s\left(g\right),\forall g,\forall t, \quad (17c)$$

$$(h_{gt}^{+})^2=-r_{st}^{+}/a_g'''+\left(p_{gt}+a_g''/2a_g'''\right)^2, s\in\Phi_s\left(g\right),\forall g,\forall t. \quad (17d)$$

In (17), h_{gt}^{+},h_{gt}^{-} are auxiliary variables.

The proof of Proposition 1 can be found in the Appendix.

Then the chance constraints in the proposed model can be summarized as the compact form as follows.

$$\Pr\left(\boldsymbol{a}^{\top}\boldsymbol{x}+\boldsymbol{b}^{\top}\boldsymbol{\xi}\leq e\right)\geq 1-\varepsilon, \quad (18)$$

where $\boldsymbol{a},\boldsymbol{b},e$ are coefficients; $\boldsymbol{x}$ and $\boldsymbol{\xi}$ are the decision and random variables, respectively.

Thanks to the results in [35], (18) can be equivalently reformulated as

$$e-\boldsymbol{a}^{\top}\boldsymbol{x}\geq G_{\boldsymbol{b}^{\top}\boldsymbol{\xi}}^{-1}\left(1-\varepsilon\right), \quad (19)$$

if the PDF of $\boldsymbol{\xi}$ admits a multidimensional GMM and $\varepsilon\leq 0.5$. In (19), G is the CDF of the random variable $\boldsymbol{b}^{\top}\boldsymbol{\xi}$ and G^{-1} represents the quantile of $\boldsymbol{b}^{\top}\boldsymbol{\xi}$ with the violation probability ε. According to [24], the CDF of $\boldsymbol{b}^{\top}\boldsymbol{\xi}$ equals to a weighted sum of the CDFs of standard Gaussian distributions, which is

$$G_{\boldsymbol{b}^{\top}\boldsymbol{\xi}}\left(y\right)=\sum_{i=1}^{I}\pi_i G_N\left(\frac{y-\boldsymbol{b}^{\top}\boldsymbol{\mu}_i}{\sqrt{\boldsymbol{b}^{\top}\boldsymbol{\Sigma}_i\boldsymbol{b}}}\right). \quad (20)$$

In (20), G_N is the CDF of standard Gaussian distribution and the rest notations are the same as (14). Given the constraint violation probability ε, the quantile can be easily calculated based on the results of DPGMM.

C. Approximations of the Quadratic Equalities

In the previous subsection, the intractable chance constraints have been converted into a set of linear inequalities and quadratic equalities. The remaining difficulties would be the nonconvex Weymouth equation (3e), the quadratic gas consumption equality of gas-fired generators (3k), and the auxiliary quadratic equalities (17c)-(17d), where the Weymouth equation suggests more computation efforts, due to the existence of absolute value signs and the quadratic equality feature. In fact, (3e) has the the Big-M based equivalent form, as shown by (21) [19].

$$M\left(\psi_{l_g t}-1\right)\leq z_{l_g^{+}t}-z_{l_g^{1}t}\leq M\left(1-\psi_{l_g t}\right),\forall l_g,\forall t, \quad (21a)$$

$$-M\psi_{l_g t}\leq z_{l_g^{+}t}-z_{l_g^{2}t}\leq M\psi_{l_g t},\forall l_g,\forall t, \quad (21b)$$

$$-M\psi_{l_g t}\leq z_{l_g^{-}t}-z_{l_g^{1}t}\leq M\psi_{l_g t},\forall l_g,\forall t, \quad (21c)$$

$$M\left(\psi_{l_g t}-1\right)\leq z_{l_g^{-}t}-z_{l_g^{2}t}\leq M\left(1-\psi_{l_g t}\right),\forall l_g,\forall t, \quad (21d)$$

$$\bar{q}_{l_g t}^2=\chi_{l_g}\left(z_{l_g^{+}t}^2-z_{l_g^{-}t}^2\right),\forall l_g,\forall t, \quad (21e)$$

where $\psi_{l_g t}$ is the binary variable; $z_{l_g^{+}t}$ and $z_{l_g^{-}t}$ are auxiliary variables representing the head and tail pressure of the actual gas flow; M is a sufficient large number. Further, (21e) can be divided into a pair inequalities as (22a) and (22b).

$$\bar{q}_{l_g t}^2+\chi_{l_g}z_{l_g^{-}t}^2-\chi_{l_g}z_{l_g^{+}t}^2\leq 0,\forall l_g,\forall t, \quad (22a)$$

$$\chi_{l_g}z_{l_g^{+}t}^2\leq\bar{q}_{l_g t}^2+\chi_{l_g}z_{l_g^{-}t}^2,\forall l_g,\forall t. \quad (22b)$$

It should be noted that (22a) is convex and can be cast into a standard SOC constraint, while (22b) is nonconvex. Therefore, the first-order Taylor expansion at the given point $\{\bar{q}_{l_g t}^{*},z_{l_g^{-}t}^{*}\}$ is employed to approximate the right side of (22b), which reads

$$\begin{aligned}&\bar{q}_{l_g t}^2+\chi_{l_g}z_{l_g^{-}t}^2\approx\left(2\bar{q}_{l_g t}^{*}\bar{q}_{l_g t}-(\bar{q}_{l_g t}^{*})^2\right)+\cdots\\&+\chi_{l_g}\left(2z_{l_g^{-}t}^{*}z_{l_g^{-}t}-(z_{l_g^{-}t}^{*})^2\right),\forall l_g,\forall t.\end{aligned} \quad (23)$$

By adding positive slack variables to the approximated counterpart of (22b), penalizing their weighted sum in the objective function, and solving a series of MISOCPs sequentially, a local optimal but feasible solution can be obtained. Similar treatment can be found in [8] and [38].

For (3k), it can be directly relaxed as the following convex inequality

$$q_{gt}\geq a_g'\lambda_{gt}+a_g''p_{gt}+a_g'''(p_{gt})^2,\forall g,\forall t, \quad (24)$$

due to the fact that the gas fuel costs are minimized in the objective function (1) [38].

The auxiliary quadratic equalities (17c)-(17d) can be converted to (25) and (26) with auxiliary variables h_{gt}' and h_{gt}'', which is similar to the treatment for equality (21e). The details of the solution feasibility recovery algorithm for quadratic equalities can be found in Algorithm 2.

$$(h_{gt}')^2+\left(p_{gt}+a_g''/2a_g'''\right)^2\leq(h_{gt}^{-})^2,\forall g,\forall t, \quad (25a)$$

$$(h_{gt}^{-})^2\leq(h_{gt}')^2+\left(p_{gt}+a_g''/2a_g'''\right)^2,\forall g,\forall t, \quad (25b)$$

$$(h_{gt}')^2\leq r_{st}^{-}/a_g''', s\in\Phi_s\left(g\right),\forall g,\forall t, \quad (25c)$$

$$r_{st}^{-}/a_g'''\leq(h_{gt}')^2, s\in\Phi_s\left(g\right),\forall g,\forall t, \quad (25d)$$

$$(h_{gt}'')^2+(h_{gt}^{+})^2\leq\left(p_{gt}+a_g''/2a_g'''\right)^2,\forall g,\forall t, \quad (26a)$$

$$\left(p_{gt}+a_g''/2a_g'''\right)^2\leq(h_{gt}'')^2+(h_{gt}^{+})^2,\forall g,\forall t, \quad (26b)$$

$$(h_{gt}'')^2\leq r_{st}^{+}/a_g''', s\in\Phi_s\left(g\right),\forall g,\forall t, \quad (26c)$$

$$r_{st}^{+}/a_g'''\leq(h_{gt}'')^2, s\in\Phi_s\left(g\right),\forall g,\forall t. \quad (26d)$$

IV. Case Study

In this section, simulation results on two test systems are provided to validate the effectiveness of the proposed methods. All tests are implemented on a laptop with Intel Core i5 and 4 GB RAM. DPGMM is coded in Python with PyMC3 and the rest are coded in MATLAB with YALMIP toolbox. The reformulated CC-OGPF model is solved by Gurobi.

A. Test System Configuration

The first test system consists of a 5-bus power network and a 7-node gas network, denoted as TS-I hereinafter. It has 1 non-gas generator, 2 gas-fired generators, 2 wind farms, 3 electrical loads, 2 gas wells, 1 compressor, 3 gas storages and 3 gas loads. The topology of TS-I is shown in Fig.3. The gas fuel of the two gas-fired generators G_1 and G_2 come from gas nodes 4 and 7, respectively. The parameters of TS-I, operation status of generators, wind generation outputs curves and the demand curves can be found in [43].

The second test system includes a modified IEEE 118-bus power network and a 48-node gas network, which is

Algorithm 2 CCP based Solution Feasibility Recovery.

1: Taking the general form of the quadratic equality as an example, it can be approximated by (27a) and (27b), where x is the one-dimension decision variable, $\boldsymbol{y}$ is the $n \times 1$ decision vector, j and t are indexes.

$$\boldsymbol{y}_{jt}^T \boldsymbol{y}_{jt} \leq x'_{jt} x''_{jt}, \forall j, \forall t, \tag{27a}$$

$$x'_{jt} x''_{jt} \leq \boldsymbol{y}_{jt}^T \boldsymbol{y}_{jt} \approx 2\boldsymbol{y}_{jt}^T \boldsymbol{y}_{jt}^0 - (\boldsymbol{y}_{jt}^0)^T \boldsymbol{y}_{jt}^0, \forall j, \forall t. \tag{27b}$$

An initial point can be obtained by solving the reformulated CC-OGPF model with (27a). Then, (27b) can be derived with the initial point.

2: Set iteration index $n = 1$. Select values for δ_1, δ_2, ρ^1, $\rho^{\max}$, $n^{\max}$ and $\kappa > 1$.

3: Set the values of $\boldsymbol{y}_{jt}^n$, ς_{jt}^n as the solution of following problem. Compared with (1), the penalty term for ς_{jt}^n has been considered.

$$F_{\text{SSA}}^n = \min \left(F + \rho^n \sum_t \sum_j \varsigma_{jt}^n \right).$$

s.t. basic constraints excluding (27b),

$$(x'_{jt})^n (x''_{jt})^n - 2(\boldsymbol{y}_{jt}^n)^T \boldsymbol{y}_{jt}^{n-1} + (\boldsymbol{y}_{jt}^{n-1})^T \boldsymbol{y}_{jt}^{n-1} \leq \varsigma_{jt}^n,$$

$$\varsigma_{jt}^n \geq 0, \forall j, \forall t.$$

4: Set $\rho^{n+1} = \min(\kappa \rho^n, \rho^{\max})$. If convergence criteria (28) and (29) are satisfied, then quit; else if $n > n^{\max}$, then quit; else, set $n = n + 1$ and go back to Step 3.

$$\left| F_{\text{CCP}}^n - F_{\text{CCP}}^{n-1} \right| \leq \delta_1, \tag{28}$$

$$\varsigma_{jt}^n \leq \delta_2 \cdot \min \left\{ \left| (x'_{jt})^n (x''_{jt})^n \right|, \left| 2(\boldsymbol{y}_{jt}^n)^T \boldsymbol{y}_{jt}^{n-1} - (\boldsymbol{y}_{jt}^{n-1})^T \boldsymbol{y}_{jt}^{n-1} \right| \right\}, \forall j, \forall t. \tag{29}$$

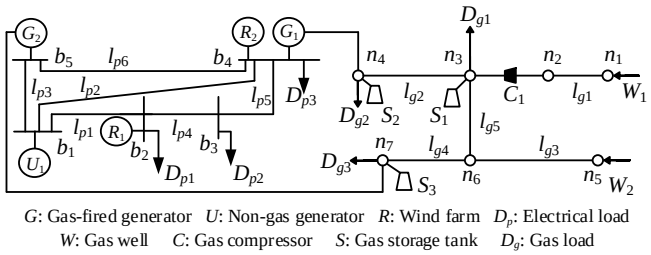

Fig. 3. Topology of TS-I.

denoted as TS-II. There are 44 non-gas generators, 10 gas-fired generators, 9 wind farms, 30 electrical loads, 9 gas wells, 8 compressors, 19 gas storages and 11 gas loads in TS-II. Refer to [43] for the topology of TS-II and the modeling parameters of CC-OGPF.

B. Simulation Results

TS-I is selected as the testbed to verify the effectiveness of the proposed methods. The number of time periods is set as $T = 24$. 3,000 samples are generated, where 2,000 of them are used to construct the reference distribution and the rest 1,000 are employed to validate the effectiveness. As there are two wind farms in TS-I, each sample is a 48-dimension vector. The constraint violation probability is selected as 5%.

1) Comparison with other uncertainty related decision-making models: Other than the adopted chance-constrained modeling approach, the scenario-based stochastic optimization (SO) and the uncertainty set based robust optimization (RO) methods are also common methods for uncertainty quantification. The scenario-based SO method proposed in [44] and the RO method proposed in [45] are reproduced for comparison, where 20 of the 2,000 training samples are randomly selected as the representative scenarios in the SO method and the boundaries of the uncertainty set in the RO method are chosen as the boundaries of training samples, respectively. The operation costs and constraint average violation rates are gathered in Table I. It can be observed that the operation costs and constraint average violation rate of the robust method are the highest and lowest, respectively, as it can provide feasibility guarantee for all the data samples, resulting in over-conservative operation strategy. The scenario-based SO method can offer the most economic operation strategy, however, its constraint violation rate is the highest, due to the limited description capability of the selected scenarios. The operation costs of the chance-constrained modeling method is moderate, as all the historical data samples are employed in constructing the uncertainty distribution.

TABLE I
SIMULATION RESULTS UNDER DIFFERENT UNCERTAINTY QUANTIFICATION METHODS.

Methods	Operation costs ($)	Average violation rate (%)
Robust	2.6227×10^6	0
Scenario-based	2.0170×10^6	12.37
Chance-constained	2.1818×10^6	5.03

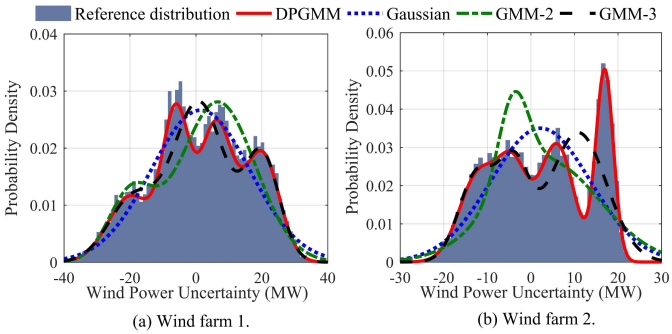

(a) Wind farm 1. (b) Wind farm 2.

Fig. 4. Fitted PDFs of the two wind farms at period 1.

2) Comparison with parametric fitting models: The fitting performances of different models are demonstrated in Fig.4, where only the PDFs of the two wind farms at period 1 are shown due to space limitation. In those two figures, GMM-2 and GMM-3 denote the Gaussian mixture model with 2 and 3 components, respectively. It can be observed that the fitted PDFs of Gaussian, GMM-2 and GMM-3 are significantly different from the histogram of reference distribution, while the PDF constructed by the DPGMM is quite close to the reference distribution. Though there are three or four observable peaks in the PDFs of the reference distribution, the component number calculated by

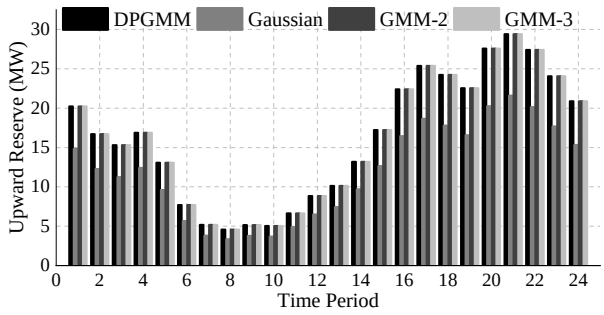

Fig. 5. Committed electrical upward reserves.

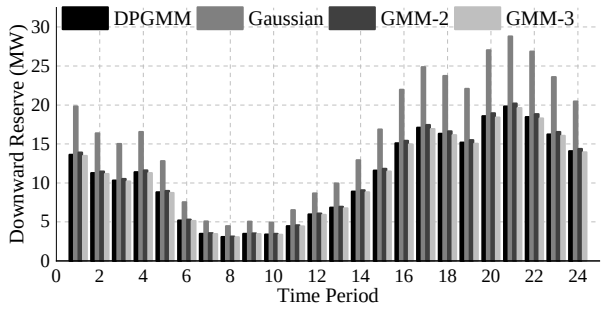

Fig. 6. Committed electrical downward reserves.

the DPGMM is 7, reflecting the difficulty of choose a proper component number for the GMM.

The numerical performances of different fitting methods are summarized in Table II. According to (14), the number of tuned parameters would grow along with the number of components in GMM, suggesting the increment of fitting time as well. The results in the second column of Table II are consistent with the above analysis. The fitting time of the DPGMM is the longest, as its component number is 7. The costs of the decisions and their aftermath are gathered in the third and fourth columns of Table II, where the performances of the DPGMM and the Gaussian distribution are the best and the worst, respectively. The reserve commitment results under the four PDFs are shown in Fig.5 and Fig.6, which explain the differences of decision costs and constraint violation probabilities. In Fig.5 and Fig.6, the reserve commitment strategy of the Gaussian distribution driven model is significantly different from the rest three, while the differences among GMM-2, GMM-3 and DPGMM are small. The last column of Table II exhibits the AIC index, which characterizes the statistical distance between the fitted distribution and the reference one. As the AIC of DPGMM is the smallest, the fitted PDF would be the "closest" to the reference distribution, resulting in fair performances in both decision costs and constraint violation probability.

TABLE II
PERFORMANCE OF DIFFERENT PDF FITTING METHODS.

Methods	Time (s)	Objective ($)	Violation rate (%)	AIC
Gaussian	0.827	2.1952×10^6	12.75	3.1644×10^4
GMM-2	1.824	2.1917×10^6	4.85	2.9637×10^4
GMM-3	2.651	2.1821×10^6	5.55	2.8956×10^4
DPGMM	7.348	2.1818×10^6	4.85	2.8167×10^4

3) The feasibility of the OGPF solution: The feasibility of the solution from the relaxed model and the proposed one is shown in Table III. It can be observed that the maximum relative gap of the relaxed solution w.r.t the original constraints, defined as (30), could be 48.41%, which is obviously infeasible. After performing the CCP based feasibility recovery algorithm, the maximum relative gap reduces to $6.55\times10^{-5}\%$, and the solution could be regarded as a feasible one, demonstrating the effectiveness of Algorithm 2.

TABLE III
SOLUTION FEASIBILITY TEST RESULTS.

Maximum relative gap (%)	
Solution of the relaxed model	Solution with feasibility recovery
48.41	6.55×10^{-5}

$$\max \left| \frac{x'_{jt}x''_{jt} - \boldsymbol{y}_{jt}^T \boldsymbol{y}_{jt}}{x'_{jt}x''_{jt}} \right| \times 100\%, \forall j, \forall t. \tag{30}$$

The iteration criterion of CCP is shown in Fig.7, where the left figure represents the iteration of the objective function and the right one represents the iteration of the relative gap defined as (30). It can be observed that the solution becomes a feasible one after three iterations, reflecting the well convergence performance of the devised algorithm.

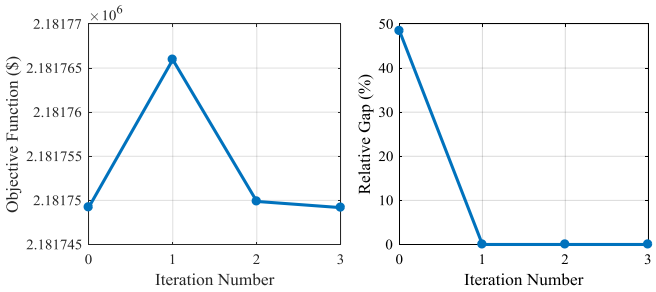

Fig. 7. Iteration criterion of CCP.

4) The necessity of considering the gas network model: Fig.8 shows the gas demands of the gas-fired generators with/without the gas network. Fig.9 shows the nodal pressure of the connecting nodes of the gas-fired generators, where the initial and terminal nodes of the gas delivery pipeline for gas-fired generator G_1 are gas nodes n_3 and n_4, respectively, and those for gas-fired generator G_2 are gas nodes n_6 and n_7, respectively. In Fig.8, the impact of the gas network on power system operation can be observed. Comparing the result without the gas network model, the gas demands from gas-fired generators would be decreased. The reason is that the operation constraints of the gas network would impose addition limitations on the operation strategy of gas-fired generators, which would affect their gas demands in return. If we take a look at the nodal pressure curves, it can be found that the pressures of the initial and terminal nodes of gas delivery line for gas-fired generation G_1 have simultaneously reached its upper and lower bounds after period 7, respectively, which leads to the maximum pressure drop and also reflects the gas delivery bottleneck. Thus, the available gas for gas-fired generator G_1 would decrease after adding the gas network model. At this moment, the nodal pressure of the gas delivery for gas-fired generator G_2 are far away from their boundaries. Therefore, its gas

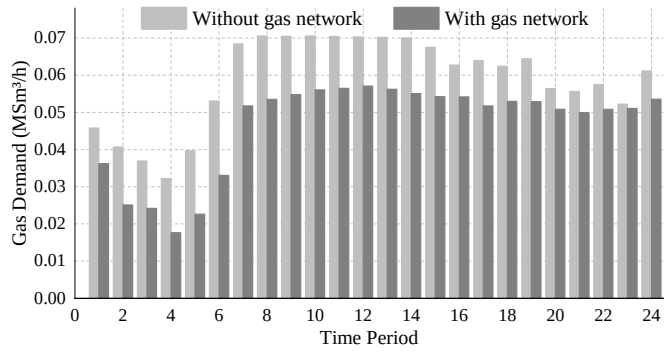

(a) Gas-fired generator G_1

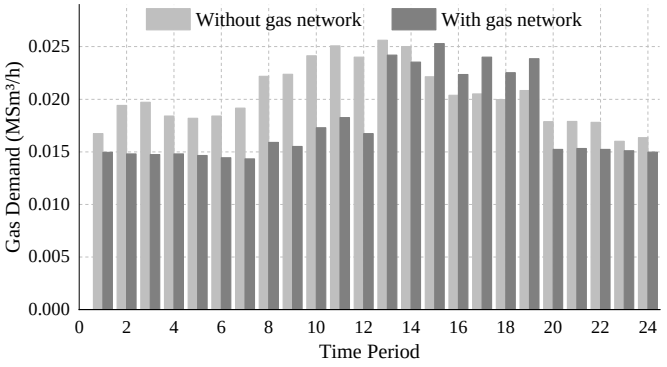

(b) Gas-fired generator G_2

Fig. 8. Gas demands of the gas-fired generators.

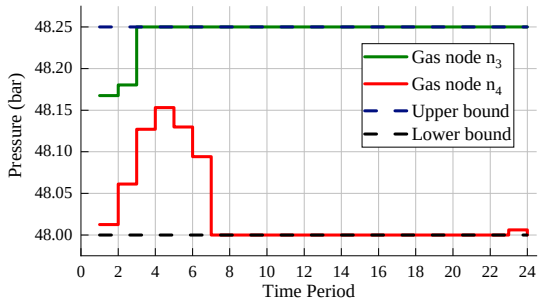

(a) Nodal pressure of the gas delivery pipeline for gas-fired generator G_1

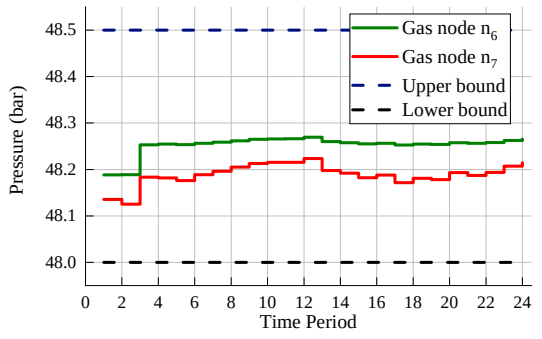

(b) Nodal pressure of the gas delivery pipeline for gas-fired generator G_2

Fig. 9. Nodal pressure of the gas delivery pipelines for gas-fired generators.

delivery is much more flexible. In some time periods, say period 15 to period 19, the consumed gas is even more after considering the gas network model, though its total consumed gas throughout the 24 periods has decreased as well.

C. The Effectiveness of the Double-track Fitting Approach

The proposed double-track PDF fitting method is implemented on a rolling-horizon decision-making case, where the time interval and the number of time periods are chosen as 5 minutes and 24, respectively, so as to coordinate with the one-short runtime of DPGMM. The simulation for the rolling-horizon operation lasts for 100 times. The initial PDF-training sample set has $2,000$ samples and the constraint violation rate is set as 5%.

Fig.10 shows the trajectory of the Gaussian component reference number from the DPGMM. It can be observed that the component number stays at 4 in the first 13 runs and becomes 6 at the 14^{th} run, reflecting the impacts of the recent accumulated data. After that, the component number starts fluctuating in the interval of $[5,\ 9]$ and stops at 6 when the simulation terminates, demonstrating the necessity of persistent run of DPGMM on the offline-track.

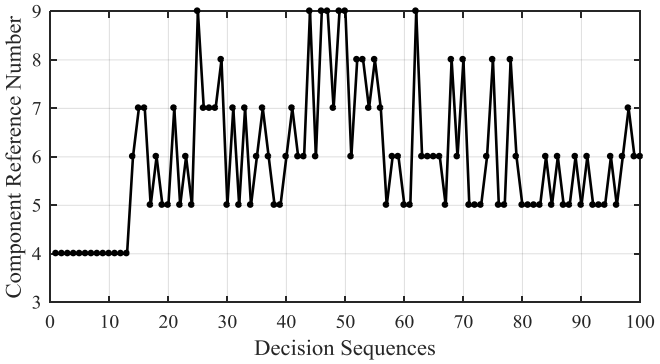

Fig. 10. The trajectory of the GMM component reference number using DP.

The constraint violation rates of the DPGMM based CC-OGPF model and the other three GMM-based ones are displayed in Fig.11, where the component numbers of GMM models are chosen as 1, 2 and 3, respectively. The constraint violation rate of the Gaussian case is always far beyond the predetermined value, which is consistent with the result in Table II. Among the other models, DPGMM-based CC-OGPF still outperforms GMM-2 and GMM-3 based ones, as it has the lowest average constraint violation rate, which is 5.26%.

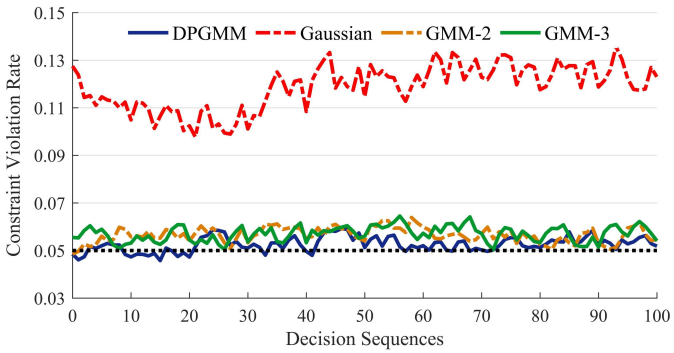

Fig. 11. Comparison of constraint violation rates during rolling-horizon decision-making.

D. Impacts of the Gas Load Uncertainty

The impact of gas load uncertainty on the upward reserves of the IEGS is shown in Fig.12, where the first three sub-figures describe the electric reserves and the last three depict the gas reserves. If the gas load uncertainty is not considered,

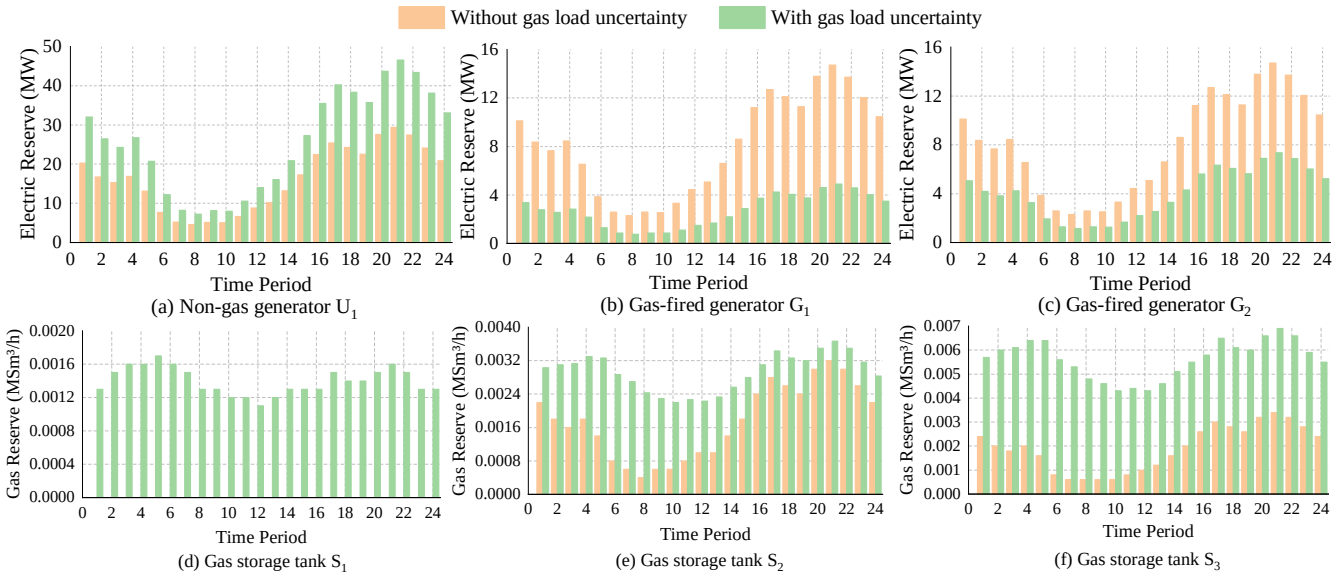

Fig. 12. Upward electric/gas reserves with/without gas load uncertainty.

there would be positive proportional relationship between the electric reserve from the gas-fired generator and the gas reserve from its connected gas storage, as reflected by the orange bars in Fig.12b & Fig.12e and Fig.12c & Fig.12f. After considering the gas load uncertainty, part of the regulation capability of gas storages would be assigned to mitigating the gas load uncertainty, resulting in the reduction of gas reserve for gas-fired generators. Accordingly, the electric reserve from gas-fired generators would decrease, and the electric reserve from the non-gas generator would increase. It should be highlighted that there is no gas-fired generator connected to gas storage S_1, therefore, the committed gas reserve in the no-gas-load-uncertainty case is zero.

E. Sensitivity Tests

1) Impacts of Violation Probability: In what follows, the impacts of violation probability on the OGPF strategy would be analyzed. In Table IV, the total costs, operation costs of the power network as well as the gas network would increase while the violation probability decreases, as the impacts of uncertainty can be broadcasted from the power network to the gas-related part through energy conversion facilities.

TABLE IV
IMPACTS OF VIOLATION PROBABILITY ON OPERATION COSTS.

Violation probability	Operation costs ($)		
	Power network	Gas network	Total
10%	7.3819×10^5	1.2426×10^6	1.9808×10^6
5%	8.4020×10^5	1.3416×10^6	2.1818×10^6
1%	1.0048×10^6	1.5001×10^6	2.5048×10^6

The violation rates of different types of constraints under different violation probability values are listed in Table V, where the values in the 2^{nd} to the 4^{th} columns are quite close to the expected violation rates. Two nontrivial observations need to be highlighted: i. the random variables affect both the line capacity and reserve constraints in an affine way and the reserve costs have been considered in the operation objective, therefore, the electrical reserve and gas storage regulation inequality constraints would be tight. However, the line capacity constraints may not be tight, which means there might be extra capacity for transmission lines when the reserve constraints become tight, resulting in smaller violation rates for line capacity constraints; ii. the violation rates for reserve and gas storage constraints are different due to the quadratic relationship between the consumed gas and outputs of the gas-fired units, which should be the same if the fuel consumption of gas-fired units is linear w.r.t. their outputs.

TABLE V
DETAILED CONSTRAINT VIOLATION RATES UNDER DIFFERENT VIOLATION PROBABILITY VALUES.

Violation probability	Violation rate (%)		
	Line capacity	Reserve	Gas storage
10%	10.10	10.31	10.86
5%	4.79	5.09	5.04
1%	0.80	1.10	1.05

2) Impacts of Sample Set Size: Three different sizes of samples are drawn from the original training data pool with 2,000 samples to construct the reference distribution, which are chosen as 300, 500, and 1,000, respectively, and all the fitted PDFs are tested by the same testing data set formed by 1,000 samples. Specifically, the smaller sample set is the subset of the larger one. The simulations are repeated 5 times and the results are gathered in Table VI.

As the sample size grows, the ranges of the violation rates of three different types of constraints decrease, which shows the performance would become more stable with more available samples. Meanwhile, the two nontrivial observations in from Table V can also be found in Table VI, confirming the effectiveness of the proposed methods.

F. Scalability Tests

The proposed methods are performed on TS-II to check their scalability. Similarly, 2,000 samples are imported to the DPGMM model and the expected constraint violation rate is selected as 5%. The simulation is repeated 20 times.

TABLE VI
IMPACTS OF SAMPLE SET SIZE ON CONSTRAINT VIOLATION RATES.

Sample Number		Violation rate (%)		
		Line capacity	Reserve	Gas storage
300	max	5.15	6.90	7.01
	mean	4.66	5.91	5.99
	min	4.23	5.14	5.26
500	max	5.04	5.87	5.95
	mean	4.63	5.18	5.28
	min	4.31	4.64	4.69
1000	max	5.03	5.99	5.94
	mean	4.61	5.13	5.27
	min	4.31	4.77	4.78

Table VII gathers algorithmic performances of solving the CC-OGPF model. It can be observed that the calculation time for a moderate test system is acceptable and the iteration number of the SOC-based algorithm in Section III.C is quite stable, revealing the promising performance of the proposed methods on real-world cases.

TABLE VII
SIMULATIONS RESULTS OF TS-II.

	Calculation time (s)	Iteration number
max	638.325	4
mean	594.596	4
min	575.278	4

The effectiveness of the proposed online-offline double-track PDF fitting method is verified by a series of 100-time sequential decision-making, where the initial data set has $2,000$ samples and the expected constraint violation rate is set as 5%. In this case, the dispatch time interval is set as 15 minutes, which is coordinated with CC-OGPF decision. The marginal PDFs of the wind farm outputs with the initial data set and the one in the 100^{th} decision at time period 1 are shown in Fig.13 and Fig.14, respectively, where only the first three wind farms with the smallest index number are shown for simplicity. It can be observed that the component numbers of Gaussian distributions have changed significantly, as the result of data accumulation, demonstrating the necessity of the proposed non-parametric PDF fitting method.

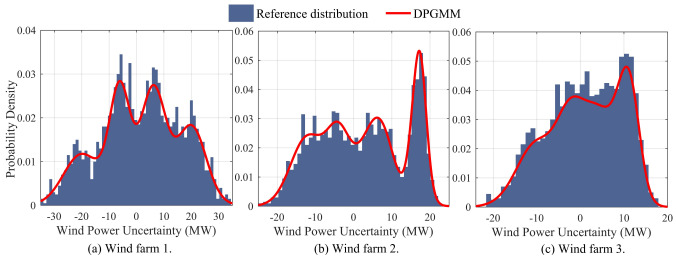

Fig. 13. The initial marginal PDFs of the first three wind farms at time period 1.

The variation curve of the Gaussian component reference number during the 100 decisions is shown in Fig.15, where the component number varies from 25 to 40. Meanwhile, no obvious monotonicity pattern can be found in this curve, as the result is completely data-driven. Therefore, it is difficult to predetermine the reference number of Gaussian distribution. The constraint violation rate curves w.r.t. the testing data set with different PDF fitting methods, namely Gaussian, GMM-2, GMM-10 and DPGMM are shown in Fig.16. Similar with the results in Fig.11, the performance of Gaussian distribution is far below expectation. The results of GMM-2, which is quite close to the DPGMM in TS-I, become worse, as component number is quite different from the DPGMM. Even if the component number is set as 10, its average performance over the 100 decisions is still worse than the DPGMM, revealing the effectiveness of the proposed PDF fitting method.

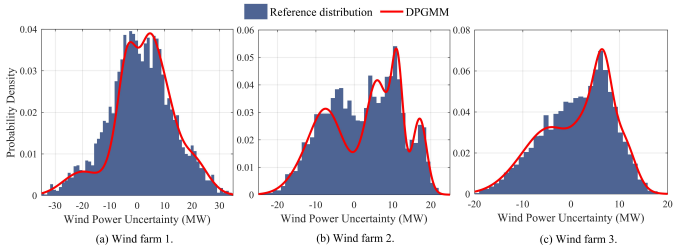

Fig. 14. Marginal PDFs of the first three wind farms at time period 1 after 100 decision sequences.

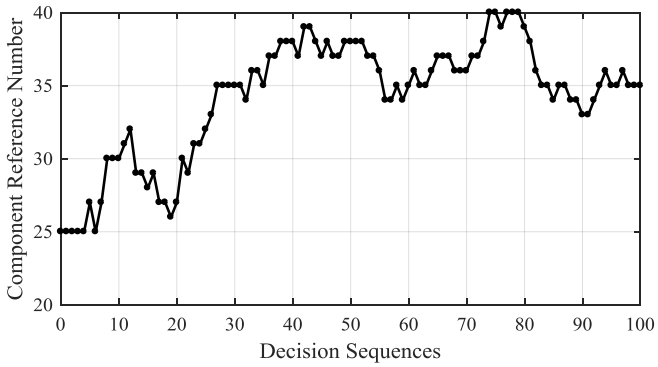

Fig. 15. The trajectory of the GMM component reference number using DP of TS-II.

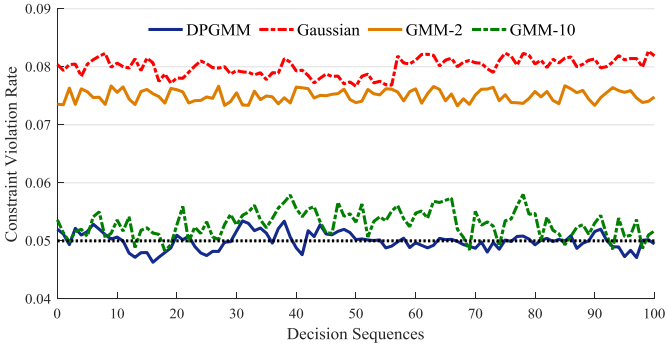

Fig. 16. Comparison of constraint violation rates during rolling-horizon decision-making of TS-II.

V. CONCLUSION

This paper addresses two vital issues which are barely discussed in the research works on CC-OGPF calculation: i. how to fit the uncertainty distribution using analytical methods in a fully data-driven manner; ii. how to deal with the difficulty of solving quadratic chance constraints originated from the quadratic gas consumption terms of gas-fired units.

To this end, a double-track online-offline uncertainty PDF fitting method is proposed, where the nonparametric feature of DPGMM and the relatively fast fitting property of the GMM are combined. The quadratic chance constraints are equivalently transformed into linear separable regular ones via reformulation and variable substitution. The remaining solution difficulties, which are the quadratic equalities, are handed over to the SOC-based convex-concave procedure. Simulation results demonstrate better uncertainty PDF fitting capability as well as closer-to-expectation operation performances of the proposed DPGMM based CC-OGPF model over the other GMM based ones. Future work would focus on developing DP-based uncertainty models to facilitate the decision-making of energy systems.

APPENDIX

Proof. According to [22] and [23], the parameters of fuel consumption functions of gas-fired generators, namely a_g''', a_g'' and a_g', are positive.

The quadratic chance constraints of gas storage actually describe the physical interdependency between the gas-fired generators and the gas network, and they originate from the random gas fuel consumption of gas-fired generators, which means both the base-case and the actual gas fuel consumption of gas-fired generators should be valid values. In other words, the outputs of gas-fired generators should be valid values, which is to say

$$\lambda_{gt}\underline{P}_g \le p_{gt},\ p_{gt} - \alpha_{gt}\Omega_t \le \lambda_{gt}\overline{P}_g, \forall g, \forall t. \tag{31}$$

Then, the non-negativity of $(p_{gt} - \alpha_{gt}\Omega_t)$ would hold according to (31). The chance constraints of gas storages could be viewed as conditional chance constraints, where the random gas fuel demands of gas-fired generator are valid values. However, it should be noted that **we do not actually require (31) hold for any random wind generation outputs.**

Combining the non-negativity of $(p_{gt} - \alpha_{gt}\Omega_t)$ and r_{st}^-, we have

$$0 \le p_{gt} - \alpha_{gt}\Omega_t + a_g''/2a_g''', \forall g, \forall t, \tag{32}$$

$$0 \le r_{st}^-/a_g''' + \left(p_{gt} + a_g''/2a_g'''\right)^2, \forall g, \forall t. \tag{33}$$

Then, one can directly take the square roots of both sides of the inequality inside the $\Pr(\cdot)$ function of (16a). Hence, (17a) and (17c) equal to (16a).

As r_{st}^+ represents the upper bound of the in-flow of gas storages due to gas consumption decrement of gas-fired generators, we have

$$\begin{aligned} r_{st}^+ &\le f_g(p_{gt}) - f_g(\lambda_{gt}\underline{P}_g) \\ &= a_g'''p_{gt}^2 + a_g''p_{gt} - a_g'''(\lambda_{gt}\underline{P}_g)^2 - a_g''\lambda_{gt}\underline{P}_g. \end{aligned} \tag{34}$$

Combining (34), the sign of the right-side of inequality inside the $\Pr(\cdot)$ function of (16b) can be obtained by the following inequality.

$$\begin{aligned} &-r_{st}^+/a_g''' + \left(p_{gt} + a_g''/2a_g'''\right)^2 \\ =&\frac{1}{a_g'''}\left(a_g'''p_{gt}^2 + a_g''p_{gt} + \frac{(a_g'')^2}{4a_g'''} - r_{st}^+\right) \\ \ge&\frac{1}{a_g'''}\left(a_g'''(\lambda_{gt}\underline{P}_g)^2 + a_g''\lambda_{gt}\underline{P}_g + \frac{(a_g'')^2}{4a_g'''}\right) \ge 0. \end{aligned} \tag{35}$$

Consequently, an equivalent form of (16b) would be available by taking the square roots of both sides of the inequality inside the $\Pr(\cdot)$ function, which is (17b) and (17d). □

REFERENCES

[1] H. Sun, Q. Guo, B. Zhang, W. Wu, B. Wang, X. Shen, and J. Wang, "Integrated energy management system: Concept, design, and demonstration in china," *IEEE Electrification Magazine*, vol. 6, no. 2, pp. 42–50, June 2018.

[2] P. Stevens, *The shale gas revolution: Developments and changes*. Chatham House London, 2012.

[3] C. Liu, M. Shahidehpour, Y. Fu, Z. Li *et al.*, "Security-constrained unit commitment with natural gas transmission constraints," *IEEE Trans. Power Syst.*, vol. 24, no. 3, pp. 1523–1536, 2009.

[4] C. Unsihuay-Vila, J. W. Marangon-Lima, A. C. Z. de Souza, I. J. Perez-Arriaga, and P. P. Balestrassi, "A model to long-term, multiarea, multistage, and integrated expansion planning of electricity and natural gas systems," *IEEE Trans. Power Syst.*, vol. 25, no. 2, pp. 1154–1168, May 2010.

[5] C. Wang, W. Wei, J. Wang, F. Liu, and S. Mei, "Strategic offering and equilibrium in coupled gas and electricity markets," *IEEE Trans. Power Syst.*, vol. 33, no. 1, pp. 290–306, Jan 2018.

[6] C. M. Correa-Posada and P. Sánchez-Martın, "Security-constrained optimal power and natural-gas flow," *IEEE Trans. Power Syst.*, vol. 29, no. 4, pp. 1780–1787, 2014.

[7] C. M. Correa-Posada and P. Sánchez-Martín, "Integrated power and natural gas model for energy adequacy in short-term operation," *IEEE Trans. Power Syst.*, vol. 30, no. 6, pp. 3347–3355, 2014.

[8] C. Wang, W. Wei, J. Wang, L. Bai, Y. Liang, and T. Bi, "Convex optimization based distributed optimal gas-power flow calculation," *IEEE Trans. Sustain. Energy*, vol. 9, no. 3, pp. 1145–1156, 2017.

[9] A. K. Prasad and S. Roy, "Reduced dimensional chebyshev-polynomial chaos approach for fast mixed epistemic-aleatory uncertainty quantification of transmission line networks," *IEEE Trans. Compon. Packag. Manuf. Technol.*, vol. 9, no. 6, pp. 1119–1132, 2019.

[10] C. Lee, J. Wu, W. Wang, and X. Yue, "Neural network gaussian process considering input uncertainty for composite structures assembly," *IEEE/ASME Transactions on Mechatronics*, pp. 1–1, 2020.

[11] C. Zhang, H. Chen, K. Shi, Z. Liang, W. Mo, and D. Hua, "A multi-time reactive power optimization under interval uncertainty of renewable power generation by an interval sequential quadratic programming method," *IEEE Trans. Sustain. Energy*, vol. 10, no. 3, pp. 1086–1097, 2019.

[12] P. Xiong and C. Singh, "A distributional interpretation of uncertainty sets in unit commitment under uncertain wind power," *IEEE Trans. Sustain. Energy*, vol. 10, no. 1, pp. 149–157, 2019.

[13] M. Lubin, Y. Dvorkin, and S. Backhaus, "A robust approach to chance constrained optimal power flow with renewable generation," *IEEE Trans. Power Syst.*, vol. 31, no. 5, pp. 3840–3849, 2015.

[14] D. Huo, C. Gu, K. Ma, W. Wei, Y. Xiang, and S. Le Blond, "Chance-constrained optimization for multienergy hub systems in a smart city," *IEEE Trans. Indus. Elect.*, vol. 66, no. 2, pp. 1402–1412, Feb 2019.

[15] X. Zhang, M. Shahidehpour, A. Alabdulwahab, and A. Abusorrah, "Hourly electricity demand response in the stochastic day-ahead scheduling of coordinated electricity and natural gas networks," *IEEE Trans. Power Syst.*, vol. 31, no. 1, pp. 592–601, Jan 2016.

[16] P. Jarventausta, P. Verho, and J. Partanen, "Using fuzzy sets to model the uncertainty in the fault location process of distribution networks," *IEEE Trans. Power Del.*, vol. 9, no. 2, pp. 954–960, 1994.

[17] Y. He, M. Shahidehpour, Z. Li, C. Guo, and B. Zhu, "Robust constrained operation of integrated electricity-natural gas system considering distributed natural gas storage," *IEEE Trans. Sustain. Energy*, vol. 9, no. 3, pp. 1061–1071, July 2018.

[18] X. Fang, H. Cui, H. Yuan, J. Tan, and T. Jiang, "Distributionally-robust chance constrained and interval optimization for integrated electricity and natural gas systems optimal power flow with wind uncertainties," *Applied Energy*, vol. 252, p. 113420, 2019.

[19] F. Liu, Z. Bie, and X. Wang, "Day-ahead dispatch of integrated electricity and natural gas system considering reserve scheduling and renewable uncertainties," *IEEE Trans. Sustain. Energy*, vol. 10, no. 2, pp. 646–658, 2019.

[20] X. Geng and L. Xie, "Data-driven decision making in power systems with probabilistic guarantees: Theory and applications of chance-constrained optimization," *Annual Reviews in Control*, vol. 47, pp. 341 – 363, 2019.

[21] S. Xu, W. Wu, Y. Yang, B. Wang, and X. Wang, "Stochastic real-time power dispatch with large-scale wind power integration and its analytical solution," *arXiv preprint arXiv:1905.09480*, 2019.

[22] M. Ž. Đurović, A. Milačić, and M. Kršulja, "A simplified model of quadratic cost function for thermal generators," in *23rd International DAAAM Symposium Intelligent Manufacturing & Automation: Focus on Sustainability*, 2012.
[23] Tao Guo, M. I. Henwood, and M. van Ooijen, "An algorithm for combined heat and power economic dispatch," *IEEE Trans. Power Syst.*, vol. 11, no. 4, pp. 1778–1784, Nov 1996.
[24] Z. Wang, C. Shen, F. Liu, X. Wu, C.-C. Liu, and F. Gao, "Chance-constrained economic dispatch with non-gaussian correlated wind power uncertainty," *IEEE Trans. Power Syst.*, vol. 32, no. 6, pp. 4880–4893, 2017.
[25] Z. Wang, C. Shen, F. Liu, J. Wang, and X. Wu, "An adjustable chance-constrained approach for flexible ramping capacity allocation," *IEEE Trans. Sustain. Energy*, vol. 9, no. 4, pp. 1798–1811, 2018.
[26] T. Campbell and J. P. How, "Bayesian nonparametric set construction for robust optimization," in *2015 American Control Conference (ACC)*. IEEE, 2015, pp. 4216–4221.
[27] C. Ning and F. You, "Data-driven adaptive robust unit commitment under wind power uncertainty: a bayesian nonparametric approach," *IEEE Trans. Power Syst.*, vol. 34, no. 3, pp. 2409–2418, 2019.
[28] W. Sun, M. Zamani, M. R. Hesamzadeh, and H.-T. Zhang, "Data-driven probabilistic optimal power flow with nonparametric bayesian modeling and inference," *IEEE Trans. Smart Grid*, 2019.
[29] C. Wang, J. Paisley, and D. Blei, "Online variational inference for the hierarchical dirichlet process," in *Proceedings of the Fourteenth International Conference on Artificial Intelligence and Statistics*. JMLR Workshop and Conference Proceedings, 2011, pp. 752–760.
[30] H. Su and T. Liu, "Enhanced-online-random-forest model for static voltage stability assessment using wide area measurements," *IEEE Trans. Power Syst.*, vol. 33, no. 6, pp. 6696–6704, 2018.
[31] V. Malbasa, C. Zheng, P. Chen, T. Popovic, and M. Kezunovic, "Voltage stability prediction using active machine learning," *IEEE Trans. Smart Grid*, vol. 8, no. 6, pp. 3117–3124, 2017.
[32] Z. Zhang, R. Yao, S. Huang, Y. Chen, S. Mei, and K. Sun, "An online search method for representative risky fault chains based on reinforcement learning and knowledge transfer," *IEEE Trans. Power Syst.*, vol. 35, no. 3, pp. 1856–1867, 2020.
[33] R. Sun, Y. Liu, and L. Wang, "An online generator start-up algorithm for transmission system self-healing based on mcts and sparse autoencoder," *IEEE Trans. Power Syst.*, vol. 34, no. 3, pp. 2061–2070, 2019.
[34] S. M. Mazhari, N. Safari, C. Y. Chung, and I. Kamwa, "A quantile regression-based approach for online probabilistic prediction of unstable groups of coherent generators in power systems," *IEEE Trans. Power Syst.*, vol. 34, no. 3, pp. 2240–2250, 2019.
[35] S. Kataoka, "A stochastic programming model," *Econometrica (pre-1986)*, vol. 31, no. 1, 2, p. 181, 1963.
[36] C. M. Correa-Posada and P. Sánchez-Martın, "Gas network optimization: A comparison of piecewise linear models," *Optimization Online*, 2014.
[37] S. Boyd and L. Vandenberghe, *Convex optimization*. Cambridge university press, 2004.
[38] Y. He, M. Yan, M. Shahidehpour, Z. Li, C. Guo, L. Wu, and Y. Ding, "Decentralized optimization of multi-area electricity-natural gas flows based on cone reformulation," *IEEE Trans. Power Syst.*, vol. 33, no. 4, pp. 4531–4542, 2017.
[39] O. Martin, *Bayesian Analysis with Python*. Packt Publishing, 2016.
[40] J. Sethuraman, "A constructive definition of dirichlet priors," *Statistica Sinica*, vol. 4, no. 2, pp. 639–650, 1994.
[41] H. Akaike, "A new look at the statistical model identification," in *Selected Papers of Hirotugu Akaike*. Springer, 1974, pp. 215–222.
[42] A. Tafsast, M. L. Hadjili, H. Hafdaoui, A. Bouakaz, and N. Benoudjit, "Automatic gaussian mixture model (gmm) for segmenting 18f-fdg-pet images based on akaike information criteria," in *2015 4th International Conference on Electrical Engineering (ICEE)*. IEEE, 2015, pp. 1–4.
[43] (2020). [Online]. Available: https://sites.google.com/site/chengwang0617/home/data-sheet/dpgmmccogpf
[44] J. Wang, M. Shahidehpour, and Z. Li, "Security-constrained unit commitment with volatile wind power generation," *IEEE Trans. Power Syst.*, vol. 23, no. 3, pp. 1319–1327, 2008.
[45] R. Jiang, J. Wang, and Y. Guan, "Robust unit commitment with wind power and pumped storage hydro," *IEEE Trans. Power Syst.*, vol. 27, no. 2, pp. 800–810, 2012.